

Anti- $E \times B$ flow field associated with a vortex formation in a partially ionized plasma

Atsushi Okamoto $\dagger\dagger$, Kenichi Nagaoka \ddagger , Shinji Yoshimura \ddagger , Jovo Vranješ \S , Mitsuo Kono \S , Shinichiro Kado \dagger and Masayoshi Y. Tanaka \ddagger

\dagger High Temperature Plasma Center, The University of Tokyo, 2-11-16 Yayoi, Bunkyo, Tokyo 113-8656 Japan

\ddagger National Institute for Fusion Science, 322-6 Oroshi, Toki, Gifu 509-5292 Japan

\S Center for Plasma Astrophysics, Celestijnenlaan 200B, 3001 Leuven, Belgium

\S Faculty of Policy Studies, Chuo University, Hachioji, Tokyo 192-0393, Japan

Abstract. A high-density magnetized plasma has been studied for understanding of plasma dynamics in partially ionized plasmas. While research of plasma dynamics on fully ionized plasma has been developed in the past century as well as on weakly ionized plasma, the understanding of partially ionized plasma is a current issue especially in considering divertor plasmas, industrial plasmas and ionosphere plasma. In this paper, the experimental result of ion flow field associated with a vortex formation in a partially ionized plasma is presented. The most remarkable result is that the direction of rotation is opposite to that of the $E \times B$ drift.

The experiments have been performed in the high density plasma experiment (HYPER-I) device at the National Institute for Fusion Science. The HYPER-I device produces a cylindrical plasma (30 cm diameter and 200 cm axial length) by electron cyclotron resonance (ECR) heating with a microwave (2.45 GHz, 80 kW maximum) launched at an open end of the chamber. The plasma density and the electron temperature are about 10^{13}cm^{-3} and 5 eV, respectively, for the operation pressure 30 mTorr (Argon), which is several ten times higher than that of usual ECR plasma experiments.

In the experimental condition described above, a tripolar vortex has spontaneously been formed. Ion flow velocity field, obtained with a directional Langmuir probe, shows that the rotational direction of each vortex is opposite to that of the $E \times B$ drift. Measurement of neutral density profile reveals that there is a steep density gradient of the neutrals around the vortex, thus inward momentum of the neutrals is generated due to the density gradient. The anti- $E \times B$ rotation is caused by the effective force attributable to radial momentum transfer from the directed neutrals to the ions with charge-exchange collision. The present experiment shows that this effective force may dominate the ambipolar-electric field and drive the anti- $E \times B$ vortical motion of ions.

1. Introduction

Understanding of plasma dynamics is an important and attractive issue in plasma physics. While research of plasma dynamics on fully ionized plasma has been developed in the past century as well as on weakly ionized plasma, recognition of common feature of dynamics observed in partially ionized plasmas becomes a current topic. Partially ionized plasma is defined as a plasma of intermediate degree of ionization between fully ionized plasma and weakly ionized plasma. The ionization degree of partially ionized plasma is typically of the order of ten percent, where adequate neutral particles and ions (and also electrons) coexist and interact with each other. Interesting phenomena related to plasma dynamics in partially ionized plasmas have been observed; for example, flow reversal has been observed in the scrape off layer of magnetically confined plasmas,[1] ion upflow in ionospheric plasma. Spatial dependence of the ionization degree[2] and the role of neutral particle itself are considered to be keys of these phenomena. We have observed another phenomenon related to plasma dynamics in a laboratory plasma with partially ionized condition. The phenomenon is spontaneous formation of a tripolar vortex. The tripolar vortex consists of an elliptic center vortex and two bean-shaped satellites, which have opposite signs of polarity of rotation to that of the center vortex, and remains stationary in time during the whole discharge period.

Recently, tripolar vortices were observed in the ocean (the Bay of Biscay) and in a rotating ordinary fluid to be self-organized from a complex initial condition,[3] and from a forced initial conditions.[4, 5] These results suggest that the tripolar vortex is a basic coherent structure in rotating fluids[6] or fluids subjected to the Coriolis force. A plasma in a magnetic field is equivalent to those fluids because the Lorentz force has the same effect as the Coriolis force, and hence it might be possible to occur a tripolar vortex in a plasma.[7]

In this paper, the experimental observation of a tripolar vortex in a magnetized partially ionized plasma is presented. A remarkable characteristic is that the tripolar vortex always appears with a deep density depression of neutral particles and is confined in its valley. The flow velocity measurements revealed that each vortex rotates in the anti- $E \times B$ direction, suggesting that there exists an effective radial force acting on the ions, which overcomes the radial electric field. We propose that the charge-exchange collisions between the ions and neutrals may produce the effective force through the net momentum transfer. When there is a strong inhomogeneity in the neutral density profile and the charge-exchange collision is dominant, a directed momentum of the flow of neutrals is brought into the ions by the charge-exchange collision, producing an effective force through the net momentum transfer. It is shown that the effective force may dominate the ambipolar electric field and drive the anti- $E \times B$ vortical motion of ions. The tripolar vortex observed in the present experiments is considered to be a neutral-induced tripolar vortex. The existence of neutral particles usually causes a dissipative effect, in which a dissipative instability[8] and a modification of the mode pattern take place.[10, 9] It is worth pointing out that the existence of neutral particles may change the ion dynamics qualitatively. In Sec. 2, the experimental setup is described, and the observation of tripolar vortex is presented in Sec. 3. The mechanism of anti- $E \times B$ rotation is given in Sec. 4.

2. Experimental Setup

The experiments have been performed in the high-density plasma experiment (HYPER-I) device at National Institute for Fusion Science.[11] The HYPER-I device consists of a cylindrical chamber (30 cm in diameter, 200 cm in axial length) and ten magnetic coils, which produce magnetic fields of 1 – 2 kG along the chamber axis. The schematic of HYPER-I device is shown in Fig. 1. Plasmas are produced and sustained by the electron cyclotron resonance (ECR) heating. A microwave of frequency 2.45 GHz is generated by a klystron amplifier (80 kW CW maximum) and is launched from an open end of the chamber, where the high-field side condition ($\omega_{ce} > \omega$, ω_{ce} : electron cyclotron frequency, ω : wave frequency) is satisfied. The magnetic field configuration is a so-called magnetic beach with the ECR point at 90 cm from the microwave injection window. An electron cyclotron wave is excited in the plasma and fully absorbed before reaching the ECR point.[12] The plasma dimension is 30 cm in diameter and 200 cm in axial length. The typical electron densities are 10^{12} cm^{-3} for the operation pressure 1×10^{-3} Torr (Argon), and 10^{13} cm^{-3} for 3×10^{-2} Torr. The electron temperature gradually decreases with increasing the operation pressure, and changes from 10 eV (1×10^{-3} Torr) to 3 eV (3×10^{-2} Torr). The microwave input power in the present experiment is ≤ 6.5 kW.

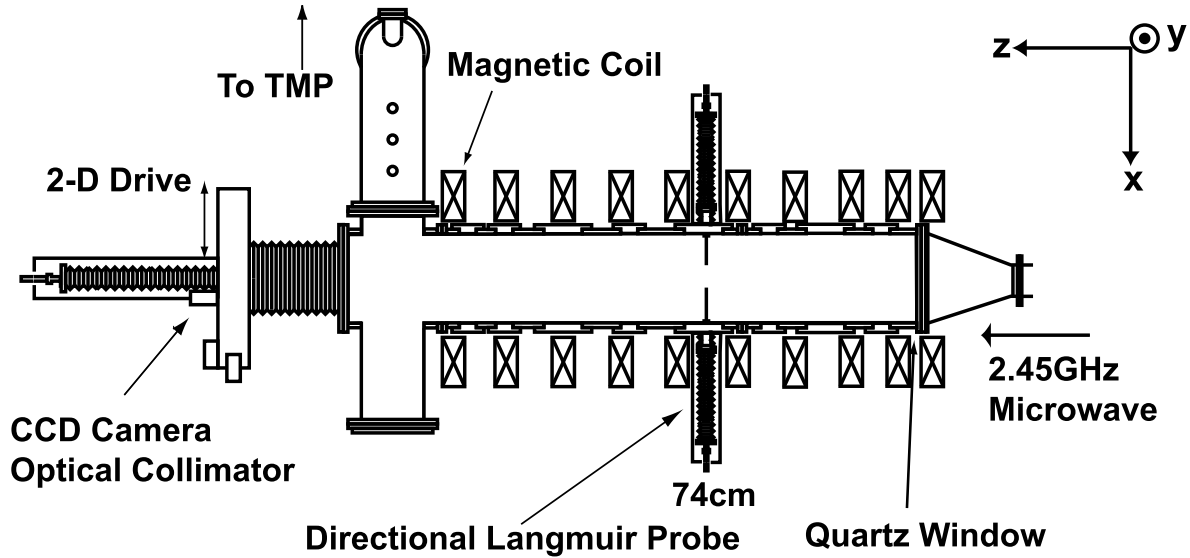


Figure 1. A schematic of the HYPER-I device

The ion flow velocities have been measured with a directional Langmuir probe (DLP), which collects a directed ion current through a small opening (1 mm diam) made on the side wall of the ceramic insulator (3 mm diam). The detailed structure of the DLP and its validity for measuring the ion flow velocity is given in Ref. [13, 14]. The flow velocity component at a certain angle θ with respect to the reference axis, $v(\theta)$, is obtained by measuring two ion saturation currents, $I_s(\theta)$ and $I_s(\theta + \pi)$, and by using the following relation:[13]

$$\frac{v(\theta)}{C_s} = \frac{1}{\alpha} \frac{I_s(\theta + \pi) - I_s(\theta)}{I_s(\theta + \pi) + I_s(\theta)}, \quad (1)$$

where θ is the angle between the normal of electrode of the DLP and the reference axis, and C_s is the ion sound speed. α is a factor of the order of unity, and is calibrated by cross-checking with other flow-measurement method such as passive[15] or laser-induced[16] spectroscopy. A two-dimensional velocity vector at a certain spatial point $\mathbf{v}(\mathbf{r})$ on a plane perpendicular to the magnetic field is determined by measuring the two components of the velocity vector. A vector field plot of the flow velocity is constructed from a data set of velocity components obtained by a pair of DLPs mounted on the radial ports located at angles $\pm 45^\circ$ from the vertical axis (see Fig. 2). The insertion angle is changed up to $\pm 34^\circ$, and the insertion chords with every 2 degrees of increment (decrement) are shown in Fig. 2. There are about 900 cross-points in the cross section, and the local velocity vectors are determined on each cross-point. The distance between the nearest cross-points is about 7 mm in the central region and about 3 – 11 mm near the chamber wall. From the original data set with the variable distances, we produce a new data set on the lattice points with equal spacing (5 mm) by interpolation, and then make the vector field plot of the flow velocity. The radial profile of density, electron temperature and space potential have been measured with a Langmuir probe.

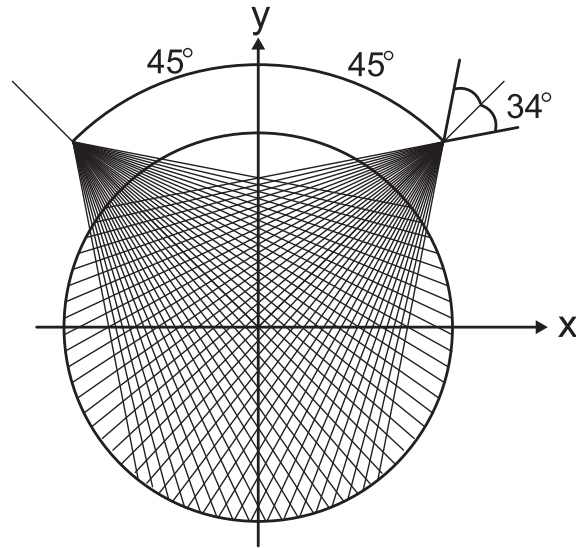


Figure 2. Insertion chords of the two-dimensional DLP system. There are about 900 cross-points, on which the flow velocity vectors are determined.

The spectroscopic measurements have been carried out to obtain the neutral density profile. A two-dimensional motor drive system with a collimated optic fiber is equipped at the end of the chamber (see Fig. 1). The focal point of the optical system is set to infinity to collect the visible light emitted to the direction parallel to the axis of the cylindrical plasma. The diameter of the viewing chord is 6 mm, and the collected light is analyzed by a spectrometer (focal length 1 m) to select a specific wavelength, and then detected by a photomultiplier tube. We have observed the emission lines from the argon ions [488.0 nm ($4p^2D^{\circ} - 4s^2P$)] and from the neutral argon [425.9 nm ($5p'[\frac{1}{2}] - 4s'[\frac{1}{2}]$)].

The intensities of emitted spectral lines from the neutrals and ions are respectively given

by $I_{\text{ArI}}(r) \propto \int n_n n_e \langle \sigma_{\text{ex}}^n v \rangle dl$ and $I_{\text{ArII}}(r) \propto \int n_i n_e \langle \sigma_{\text{ex}}^i v \rangle dl$, where dl is the distance along the line of sight, $\langle \sigma_{\text{ex}}^j v \rangle$ ($j = n, i$) are the rate coefficients of excitation process for the neutrals and ions, respectively. When the radial density profiles of plasma and neutral particles are axially uniform, the observed intensities $I_{\text{ArI}}(r)$ and $I_{\text{ArII}}(r)$ are proportional to the quantities $n_n n_e$ and $n_i n_e \approx n_e^2$, respectively. Then the ratio of $I_{\text{ArI}}(r)$ to the square root of $I_{\text{ArII}}(r)$ is proportional to the neutral density:

$$\frac{I_{\text{ArI}}(r)}{\sqrt{I_{\text{ArII}}(r)}} \propto n_n(r). \quad (2)$$

We assume here the uniform profiles along the plasma axis, which will be justified by the experimental results.

3. Observation of Tripolar Vortex

End-view images of the plasma taken by a CCD camera for the different operation pressures are shown in Fig. 3, where Fig. 3(a) is for 6.7×10^{-3} Torr and Fig. 3(b) for 2.5×10^{-2} Torr. At the pressure 6.7×10^{-3} Torr (and lower than this pressure), the plasmas are uniformly produced over the whole cross section of the vacuum chamber. At the operation pressure 2.5×10^{-2} Torr, the two bright and bean-shaped regions appear in the central part of the plasma, between which there is a dark elliptic region. The diameter of the whole structure is about 15 cm, which is about one half of the diameter of the plasma filling in the vacuum chamber. This structure is spontaneously formed when the microwave is turned on, and remains stationary in time during the whole discharge period (~ 30 s).

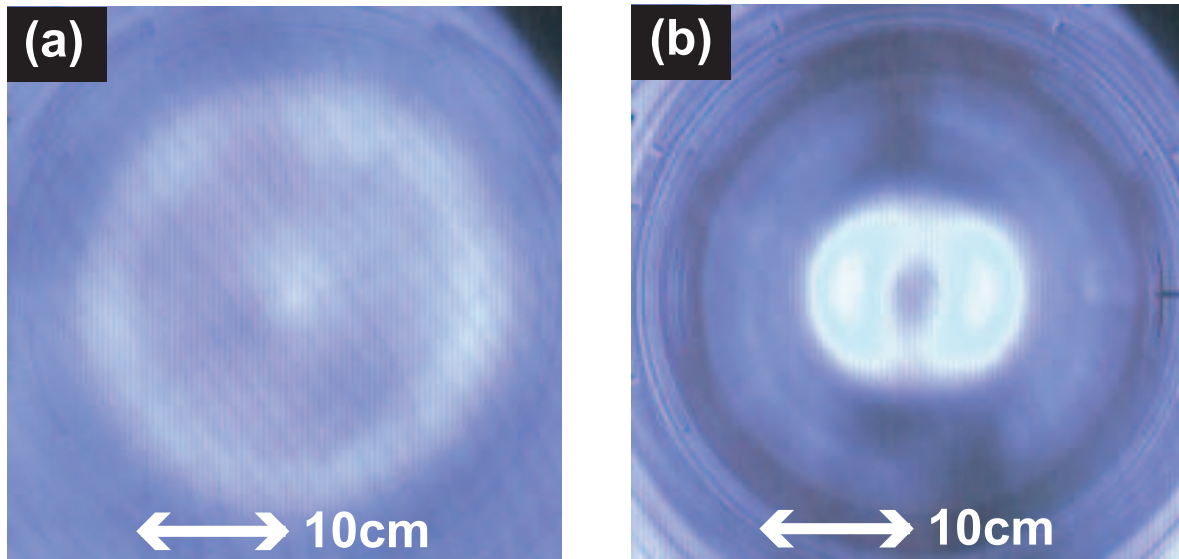


Figure 3. End-view images of the plasma for different operation pressures. (a): 6.7×10^{-3} Torr, (b): 2.5×10^{-2} Torr.

The radial profiles of the ion and neutral densities have been measured along the horizontal center chord ($y = 0$) for the same operation pressures as in Fig. 3, and the results

are shown in Fig. 4. The ion density profiles measured with a Langmuir probe are indicated in the top [Figs. 4(a) and 4(c)] and the corresponding neutral density profiles determined by Eq. (2) in the bottom [Figs. 4(b) and 4(d)]. The ion density profile determined by the optical measurement, which is given by $n_i(r) \propto \sqrt{I_{\text{ArII}}(r)}$, is also shown in Fig. 4(c) to cross-check the validity of the optical method. The calibration factor for the optical measurement is determined so as to give the equal value of $n_i(r)$ at the point $r = 10$ cm. There is a good agreement between the two. Since the optical measurement provides a line-integrated quantity, this agreement suggests that the observed structure is axially homogeneous. In fact, we have confirmed by the Langmuir probe measurement that the observed structure is axially homogeneous at least more than 90 cm. It has also been confirmed that the bean-shaped bright regions shown in Fig. 3(b) are the ion density clumps.

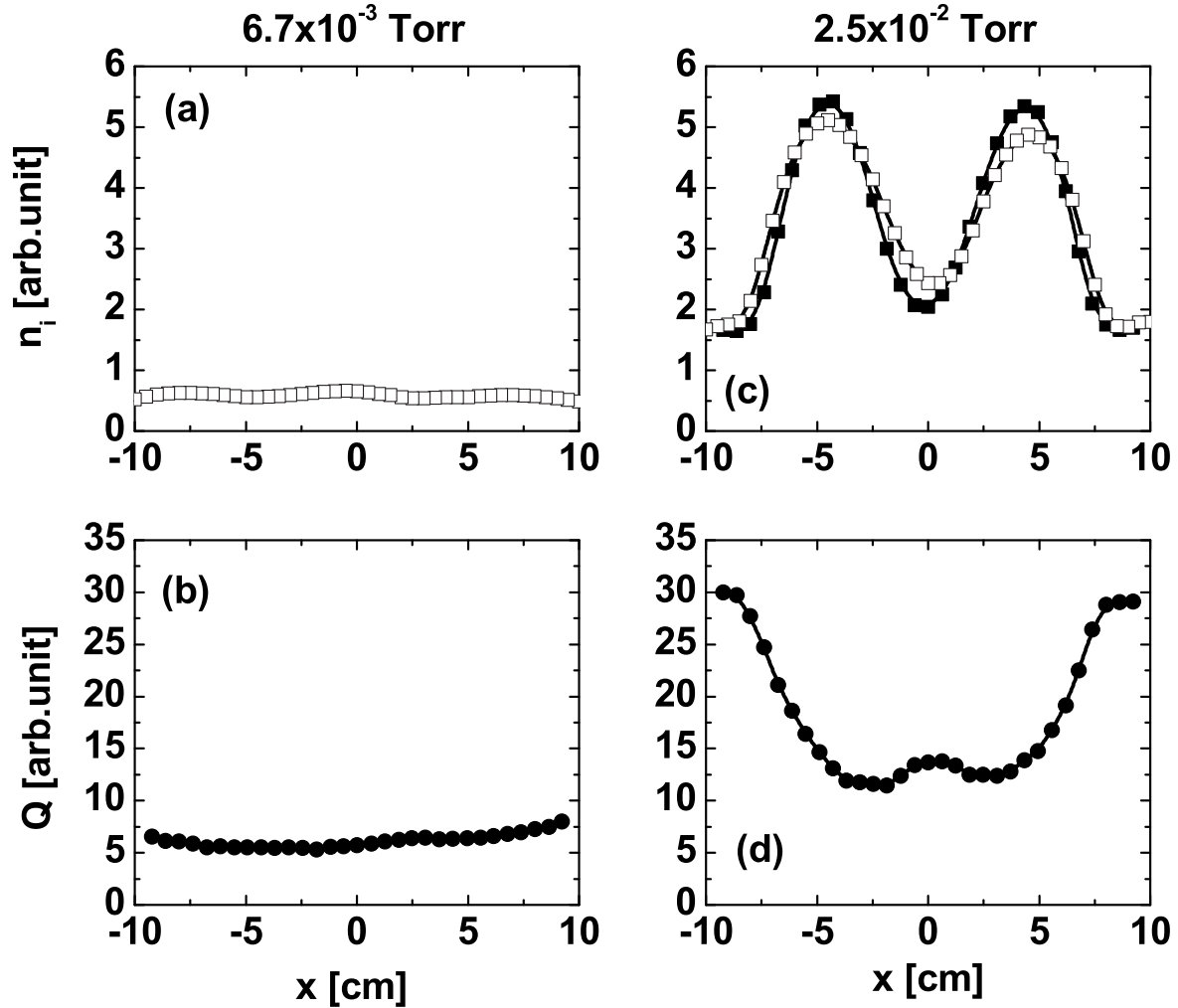


Figure 4. Ion density profiles (top) and neutral density profiles (bottom). The operation pressures are the same as in Fig. 3. In Fig. 4(c), the ion density obtained from the optical measurement is indicated by closed square (\blacksquare), and the ion density measured with a Langmuir probe by open square (\square). In Figs. 4(b) and 4(d), the quantity Q is defined as $Q = I_{\text{ArI}}(r) / \sqrt{I_{\text{ArII}}(r)} \propto n_n$.

In accordance with the appearance of bright spots, a neutral density depression occurs in the central region of the plasma [Fig. 4(d)]. It should be emphasized that when the double-peaked structure is generated in the ion density profile, the neutral density profile becomes a double-minimum distribution as shown in Fig. 4(d). Moreover, there is a close relation between the positions of the steepest density gradient of the ions and the neutrals. The width of ion clump and that of neutral depression exhibit a quite well agreement, suggesting that the observed ion density structure is confined in the neutral density depression, and there might be a dynamical coupling between the two.

The vector field plot of the ion flow velocity and the vorticity distribution[17] for a double-peaked structure are shown in Fig. 5. Figure 5(a) indicates the flow velocity field with the contour map of ion density in the background, and Fig. 5(b) the distribution of z -component of vorticity, which is constructed from the velocity data by using the following equation: $\omega = (\text{rot}v)_z \simeq \oint v_{\perp} \cdot dl / \Delta S$. In this calculation, the path of integration is so chosen to pass through the four velocity vectors on the minimum lattice points of the velocity field, and ΔS is the area surrounded by the integration path. As seen in Fig. 5(a), there are two clockwise vortical motions in both sides, which correspond to the ion density clumps. Between these clumps, there presents a counterclockwise motion whose center is a little bit shifted upward. Since the velocity field pattern is a superposition of vortical motion and other flows such as the diffusive flux, the vorticity distribution contour is much more useful to recognize the existence of vortices.[18] Figure 5(b) clearly shows the existence of three vortices; one vortex locates in the center with a positive polarity (counterclockwise rotation) and two satellites in the both sides with negative polarities (clockwise rotation). Therefore, the observed flow structure is a tripolar vortex.[19] Tripolar vortices have been already found in ordinary fluids. Unlike these vortices in ordinary fluids,[4, 5] which slowly rotate as a whole, the global vortex pattern in the plasma is stationary in the laboratory frame, which suggests that there exists a vortex solution with zero eigenfrequency. The existence of stationary tripolar solution in a plasma has been shown in Ref. [20].

4. Mechanism of Anti- $E \times B$ rotation

The electrostatic potential measurements revealed that the potential profile along the horizontal chord ($y = 0$) is a double-peaked one, and the half of the profile is shown in Fig. 6, in which the corresponding neutral density profile is also depicted. In evaluating the neutral density $n_n(r)$, the effect of temperature variation along the horizontal chord ($\delta T_e / T_e \simeq 0.1$) on the atomic cross section is taken into account. As seen in the figure, the peak position of the potential ($x \simeq 5\text{cm}$) coincides with that of ion density, and its profile is convex around the density peak, and concave near the center axis. This means that the expected $E \times B$ rotations due to this potential profile are counterclockwise for the satellite vortices, and clockwise for the core vortex, which are apparently opposite to the experimental observations. There should be a radially inward force (or momentum transfer) to explain the observed rotation of ions. The probable mechanism of generation of inward force is a net momentum transfer between the ions and neutrals. As shown in Fig. 4, a steep density gradient in the neutrals coexists with

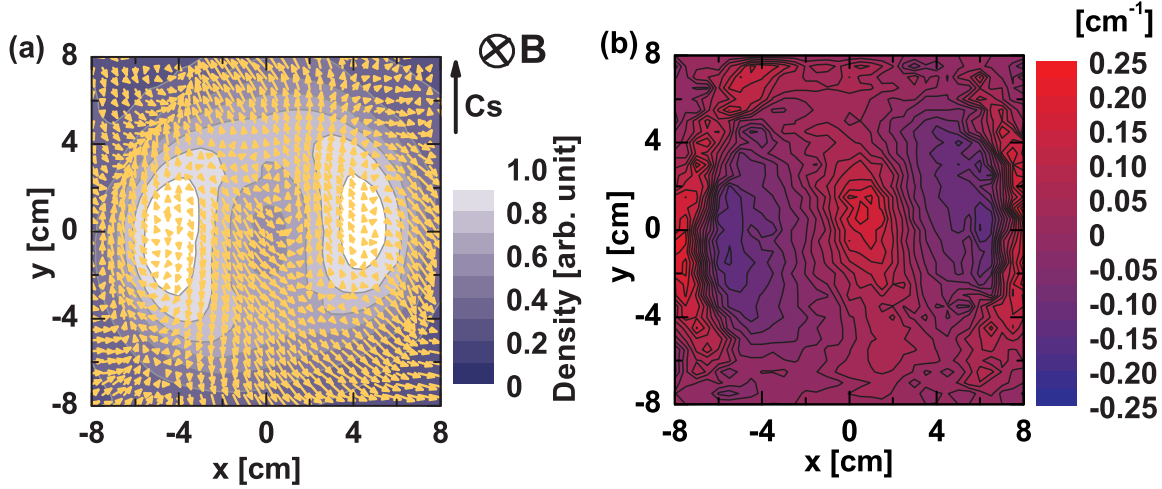


Figure 5. (a): Vector field plot of the ion flow velocity and the density contour (background). The direction of the magnetic field is indicated in the upper right of the figure. The magnitude of flow velocities are normalized by the ion sound speed, which is also indicated in the upper right of the figure. (b): Contour plot of the z -component of vorticity.

the tripolar vortex. In this circumstance, there is a directed flow of neutrals induced by the neutral density gradient, which may be given by

$$\mathbf{v}_n = -D_{\text{eff}} \nabla \log n_n, \quad (3)$$

where n_n is the density of neutrals. Since the mean free path of neutrals is comparable to the scale of vortex, we introduce an effective coefficient D_{eff} to include the enhancement factor. When the charge-exchange interaction is dominant, the directed flow of neutrals may become a source of inward momentum, i.e., during unit time interval, a momentum $P_{n \rightarrow i} = \nu_{ni} M n_n v_n$ (ν_{ni} : charge-exchange collision frequency of neutrals with ions) is brought into the ion fluids, while in the same interaction the ions lose a momentum $P_{i \rightarrow n} = \nu_{in} M n_i v_i$ (ν_{in} : charge-exchange collision frequency of ions with neutrals), resulting in a net momentum transfer. Under the present experimental conditions, the magnitude of $P_{i \rightarrow n}$ and $P_{n \rightarrow i}$ might be in the same order of magnitude. The ion momentum equation is then written as[20]

$$M n_i \left[\frac{\partial \mathbf{v}_i}{\partial t} + (\mathbf{v}_i \cdot \nabla) \mathbf{v}_i \right] = e n_i (\mathbf{E} + \mathbf{v}_i \times \mathbf{B}) - \nabla p_i - \nu_{in} M n_i (\mathbf{v}_i + D_{\text{eff}} \nabla \log n_n), \quad (4)$$

where $\nu_{ni} n_n = \nu_{in} n_i$ is used. The perpendicular velocity component is given by

$$\mathbf{v}_\perp = \frac{1}{\omega_{ci}^2 + \nu_{in}^2} \left[\frac{e}{M} (\omega_{ci} \mathbf{e}_z \times \nabla_\perp \phi - \nu_{in} \nabla_\perp \phi) + \nu_{in}^2 (\omega_{ci} \mathbf{e}_z \times \nabla_\perp \log n_i - \nu_{in} \nabla_\perp \log n_i) + (\omega_{ci} \nu_{in} D_{\text{eff}} \mathbf{e}_z \times \nabla_\perp \log n_n - \nu_{in}^2 D_{\text{eff}} \nabla_\perp \log n_n) \right], \quad (5)$$

where ω_{ci} is the ion cyclotron frequency. In deriving the above equation, the convective term $\mathbf{v} \cdot \nabla \mathbf{v}$ is omitted for simplicity, which is justified when the ion flow velocity is less than the ion sound speed. On the horizontal chord ($y = 0$), $\partial/\partial r \gg (1/r)\partial/\partial \theta$ holds, and hence the

azimuthal velocity at $y = 0$ has the simplest form to be compared with the observed velocity, which is written as

$$\frac{v_y}{C_s} = \frac{\omega_{ci} C_s}{\omega_{ci}^2 + \nu_{in}^2} \left[\frac{\partial}{\partial r} \left(\frac{e\phi}{T_e} \right) + \frac{T_i}{T_e} \frac{\partial}{\partial r} (\log n_i) + \frac{D_{\text{eff}}}{C_s^2 / \nu_{in}} \frac{\partial}{\partial r} (\log n_n) \right]. \quad (6)$$

The first term represents the $E \times B$ drift, the second term the diamagnetic drift, and the third term the $F \times B$ drift due to the "effective pressure of neutrals". The diamagnetic drift velocity is small compared with the $E \times B$ drift velocity because $T_i/T_e \ll 1$.

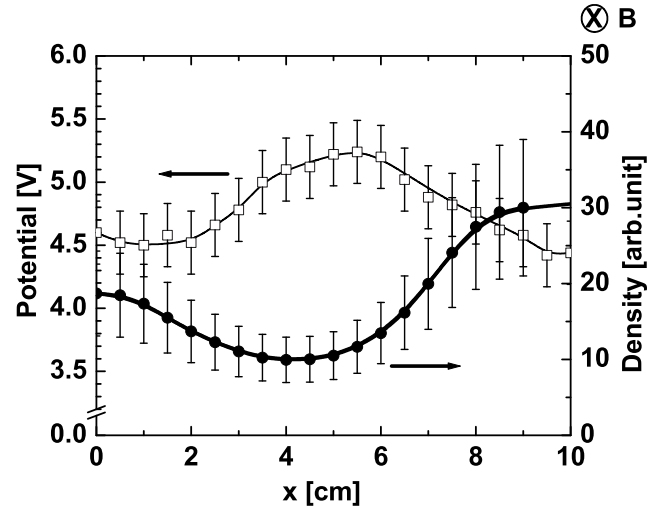


Figure 6. Electrostatic potential (\square) and neutral density profile (\bullet) of the tripolar vortex. The direction of the magnetic field is indicated in the upper right of the figure.

Figure 7 shows the azimuthal velocity profile along the horizontal chord ($y = 0$), where the bold solid line indicates the velocity obtained with the DLP. The $F \times B$ drift velocity due to the density gradient of neutrals, which is determined by the third term of Eq. (6) is also plotted in Fig. 7(a), where $D_{\text{eff}} = 5D_c$ (D_c : collisional diffusion coefficient) is used; in evaluating the absolute value of neutral density at the tripolar vortex region from the operation pressure measured at the chamber wall, there is uncertainty of density depression. This corresponds to an enhancement factor of several for D_c determined by the operation pressure. In Fig. 7, we take $D_{\text{eff}} = 5D_c$ as one example. For comparison, the $E \times B$ drift velocity given by the first term of Eq. (6) with the observed potential profile is shown in Fig. 7(b). In evaluating the $F \times B$ drift, we used the charge-exchange cross section given by Chanin,[21] and three different curves corresponding $T_e/T_n = 10, 20, 50$ are depicted. Although there remains a certain ambiguity, Fig. 7(a) shows a fairly good agreement between the experimental observation and the $F \times B$ drift due to the density gradient of neutrals. It is emphasized that the $E \times B$ drift velocity determined by the potential profile is opposite in direction [Fig. 7(b)].

In the low pressure operations, however, the neutral particle depression and thus the steep density gradient were not generated. The observed azimuthal velocity in this case well agrees with that determined by the $E \times B$ drift,[13] which is shown in Fig. 8. It is interesting to note that the central region very weakly rotates compared with the peripheral region, and there is

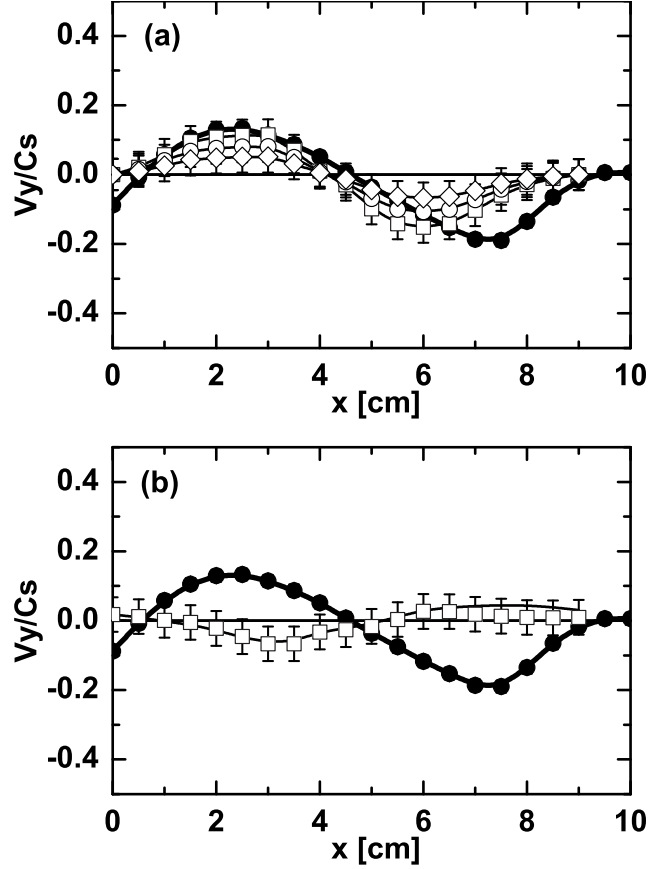


Figure 7. Comparison between the azimuthal ion velocity measured with a DLP (bold solid line) and (a) the $F \times B$ drift velocity due to the neutral density gradient (\square, \circ, \diamond), and (b) the $E \times B$ drift velocity determined from the potential profile (\square). Note that the direction of $E \times B$ drift is opposite to the observed direction of rotation. In Fig. 7(a), the drift velocities for three different neutral temperatures are plotted (\square : $T_e/T_n = 10$, \circ : $T_e/T_n = 20$, \diamond : $T_e/T_n = 50$).

a shear between the two regions ($r = 4 - 5$ cm), the position of which roughly coincides with that of the center of satellite vortex (see Fig. 4 and 5).

We can conclude that the anti- $E \times B$ rotation is attributable to the effective force originated from the density gradient in neutrals. The critical condition that the effective force overcomes the electrostatic force may be given by $en_i E \approx v_{in} M n_i D_{eff} \nabla \log n_n$. Introducing $E \sim \phi/a$ (a : plasma radius) and $\nabla \log n_n \sim l_{cx}^{-1}$ (l_{cx} : mean free path of charge-exchange collision), and using the appropriate values for other quantities, we have $l_{cx}/a \sim (e\phi/T_e)^{-1} (\sigma_{in}/\sigma_{nn}) \sqrt{T_n/T_e} \approx 0.6 - 1.4$, where $D_{eff} = 5D_c$ is assumed. Experimentally, the pressure range of the transition to the tripolar vortex is $0.7 - 1.3 \times 10^{-2}$ Torr, which corresponds to $l_{cx}/a \sim 2 - 3$, showing a rough agreement with the above estimation.

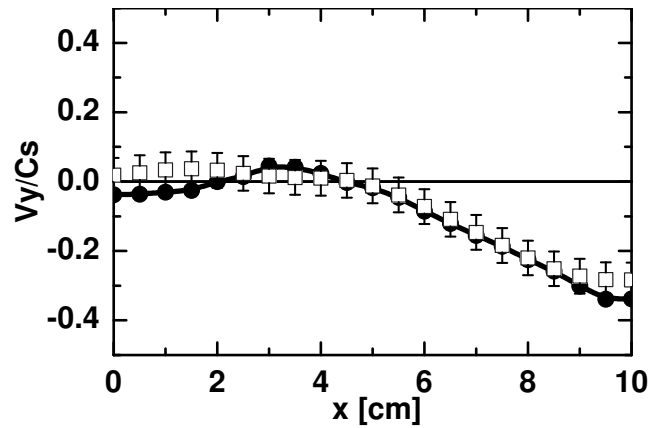


Figure 8. Comparison between the azimuthal ion velocity measured with a DLP (bold solid line) and the $E \times B$ drift velocity (\square) for the low pressure case (6.7×10^{-3} Torr).

5. Conclusion

A tripolar vortex has been observed in a magnetized plasma for the first time. The tripolar vortex coexists with a deep density hole of neutrals, and the rotation direction is opposite to that of the $E \times B$ drift. When a steep density gradient of neutrals is present, a net momentum transfer may take place through the charge-exchange interaction, producing an effective force acting on the ion fluids. Our experiment shows that this effective force may overcome the radial electric field, and generates an anti- $E \times B$ rotation. Since the existence of neutrals usually brings a dissipation term into the equation of motion, it is of importance to note that the existence of neutrals may qualitatively change the dynamical behavior of ions. The present result will be important in considering plasma behavior in partially ionized plasmas such as ionospheric plasmas and surface plasmas in confined systems.

Reference

- [1] N. Asakura, S. Sakurai, M. Shimada, Y. Koide, N. Hosogane, K. Itami, *Phys. Rev. Lett.* **84**, 3093 (2000).
- [2] J. Vranješ, M. Y. Tanaka, M. Kono, and S. Poedts, *Phys. Plasmas* **11**, 4188 (2004).
- [3] R. D. Pingree and B. L. Cann, *J. Geophys. Res.* **97**, 14353 (1992).
- [4] G. J. F. van Heijst and R. C. Kloosterziel, *Nature* **338**, 569 (1989).
- [5] G. J. F. van Heijst, R. C. Kloosterziel, and C. W. M. Williams, *J. Fluid Mech.* **225**, 301 (1991).
- [6] Z. Kizner, and R. Khvoles, *Phys. Rev. E* **70**, 016307 (2004).
- [7] J. Vranješ, G. Marić, and P. K. Shukla, *Phys. Rev. E* **61**, 7009 (2000).
- [8] F. F. Chen, *Introduction to Plasma Physics and Controlled Fusion*, 2nd ed, (Plenum, New York, 1983), pp. 218-223.
- [9] M. Kono and M. Y. Tanaka, *Phys. Rev. Lett.* **84**, 4369 (2000).
- [10] M. Y. Tanaka and M. Kono, *J. Plasma Fusion Res. SERIES* **4**, 131 (2001).
- [11] M. Y. Tanaka, M. Bacal, M. Sasao, and T. Kuroda, *Rev. Sci. Instrum.* **69**, 980 (1998).
- [12] M. Tanaka, R. Nishimoto, S. Higashi, N. Harada, T. Ohi, A. Komori, and Y. Kawai, *J. Phys. Soc. Jpn.* **60**, 1600 (1991).
- [13] K. Nagaoka, A. Okamoto, S. Yoshimura, and M. Y. Tanaka, *J. Phys. Soc. Jpn.* **70**, 131 (2001).
- [14] A. Okamoto, S. Yoshimura, and M. Y. Tanaka, *J. Plasma Fusion Res. SERIES* **6**, in press.

- [15] S. Kado, T. Shikama, S. Kajita, T. Oishi, and S. Tanaka, *Contrib. Plasma Phys.* **44**, 656 (2004).
- [16] A. Okamoto, S. Yoshimura, S. Kado, and M. Y. Tanaka, to be published in *J. Plasma Fusion Res.*
- [17] K. Nagaoka, A. Okamoto, S. Yoshimura, M. Kono, and M. Y. Tanaka, *Phys. Rev. Lett.* **89**, 075001 (2002).
- [18] A. Okamoto, K. Hara, K. Nagaoka, S. Yoshimura, J. Vranješ, M. Kono, and M. Y. Tanaka, *J. Plasma Fusion Res.* **78**, 1143 (2002).
- [19] A. Okamoto, K. Hara, K. Nagaoka, S. Yoshimura, J. Vranješ, M. Kono, and M. Y. Tanaka, *Phys. Plasmas* **10**, 2211 (2003).
- [20] J. Vranješ, A. Okamoto, S. Yoshimura, S. Poedts, M. Kono, and M. Y. Tanaka, *Phys. Rev. Lett.* **89**, 265002 (2002).
- [21] L. M. Chanin and M. A. Biondi, *Phys. Rev.* **106**, 473 (1957).